Università degli Studi di Padova

Dipartimento di Fisica e Astronomia Galileo Galilei

University of Padua - Department of Physics and Astronomy
Course: Physics Laboratory
Academic year: 2021-22

Group 13
Vittoria Pavanello - 2055706 - vittoria.pavanello@studenti.unipd.it
Riccardo Triozzi - 2055705 - riccardo.triozzi@studenti.unipd.it
Nicola Zancopè - 2053347 - nicola.zancope@studenti.unipd.it

Laboratory days: 03-08/11/2021

Study of Compton Scattering

Contents

1 Introduction

The *Compton scattering* is a process in which a photon characterized by an energy of the order of $o(1\text{ MeV})$ interacts with an electron in matter. The process is schematized in Figure 1, with the initial electron considered at rest. It is possible to derive the energy of the diffused photon, that results

$$E_f = \frac{E_i}{1 + \frac{E_i}{m_e c^2}(1 - \cos\theta)} \tag{1}$$

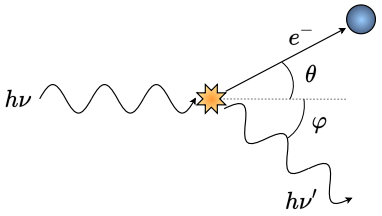

Figure 1: Scheme of the Compton scattering.

in which E_i is the energy of the incoming photon. It is worth noticing that for $\theta = 0°$ the scattered photon retains all the available energy; on the other hand, at $\theta = 90°$, the scattered electron and photon have the same energy. In general, the energy of the scattered electron is $E_e = E_i - E_f$, due to energy conservation. Finally, the aim of the experiment is:

1. to verify the energy versus angle relation for the diffused photon;

2. to measure the differential cross section at fixed angle.

2 Experimental Setup

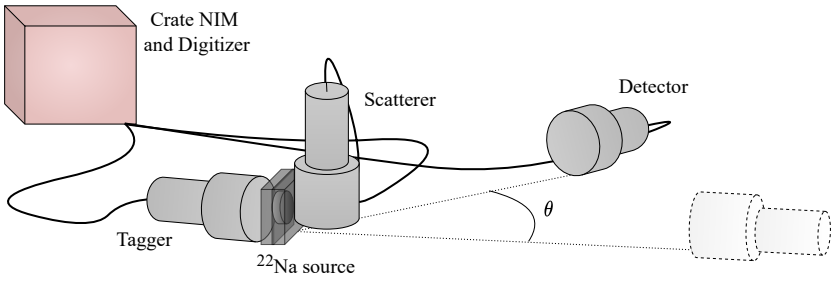

Figure 2: Scheme of the experimental setup.

The experiment exploits a radioactive ^{22}Na source, collimated by a lead brick in order to produce a well-shaped beam of photons. The activity of the source is $\mathcal{A} \sim 110$ kBq[1]. In particular, the source emits three photons, two of energy 511 keV and on at 1275 keV; the two 511 keV photons are due to the pair annihilation of the positron emitted in a β^+ decay with an electron. The beam eventually strikes a target that also works as a detector, denoted as 'Scatterer'. The Scatterer consists of a vertical, cylindrical NaI(TI) scintillator with a base diameter of 7.50 ± 0.04 cm and height of 7.50 ± 0.04 cm[2]. To properly select the photons that hit the Scatterer, the beam is tagged by using the coincidence with a second 511 keV photon detected by another detector, named 'Tagger'. The Tagger is similar to the Scatterer, consisting of a NaI(TI) scintillator with the same dimension. The diffused photon can be ultimately revealed by another similar NaI(TI) scintillator, denoted as 'Detector'. The apparatus is placed on a rotating arm that allows to move the Detector at different angular positions, within the $(0°-90°)$ range. Finally, the Detector is placed on a guideway that enables to vary the distance between Scatterer and Detector. In particular, the distance between Tagger and source was fixed at $D_1 = 3 \pm 1$ cm[3], while source and Detector were distant $D_2 = 37 \pm 1$ cm. Furthermore, the distance between source and Scatterer was $D_3 = 5 \pm 1$ cm.

[1] Source: http://www.dfa.unipd.it/fileadmin/servtec/Sorgenti_polo_sett_2021_01.pdf.

[2] Lengths' uncertainties are obtained exploiting the triangular distribution on 1 mm resolution.

[3] Only for detectors' distances errors are chosen so large because of the impossibility in precisely approaching the source while measuring.

2.1 The Electronics Chain

The detectors are supplied by fixed High Voltage (HV) values of 600 V, via the CAEN N1470 HV module. To set up the acquisition, Nuclear Instrument Modules (NIMs) were employed. The anode output is connected to the Quad Linear Gate Fan-In Fan-Out (FIFO) Philips 744, used for signal doubling. One of the signals is redirected into the DAQ system, given by the CAEN DT5720 digitizer module. The other signal is instead led to the Constant Fraction Discriminator (CFD) module, that allows to have both delayed and prompt outputs with variable delay and width. Finally, the coincidence between different detectors is achieved by using the 32-Inputs SEN Logic Unit (LU) 278 module. By selecting the appropriate 'fold' option[4], the output of this module becomes the trigger for the acquisition.

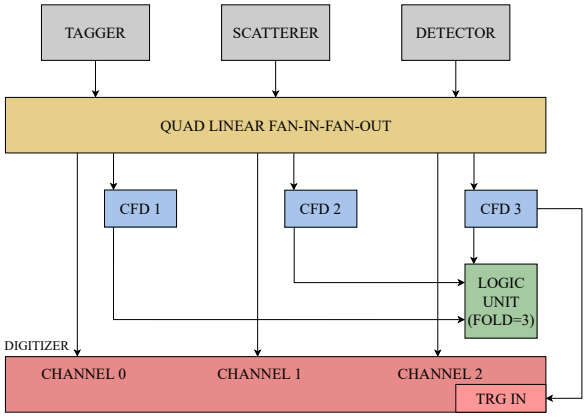

Figure 3: Scheme of the electronics setup.

Estimate of the Counting Rate The *counting rate* is the number of expected events per second and can be estimated through geometrical and physical considerations and then compared to the number displayed on the CAEN Quad Scaler module. In particular, since the collimators restrict the beam to a section with diameter $d_b \sim 3.5$ cm and area $A_{\text{sec}} = \pi d_b^2$, one can compute the ratio between A_{sec} and the total area of isotropic emission $A_{\text{tot}} = 4\pi D^2$. The counting rate can be thus computed as $r = \frac{A_{\text{sec}}}{A_{\text{tot}}} n_\gamma$. The latter term represents the amount of photons emitted per second, namely $n_\gamma = \mathcal{A} N_\gamma$ with $\mathcal{A}$ activity of the source and $N_\gamma = 3\ \frac{\gamma}{\text{decay}}$ number of photons emitted per decay. For instance, let's consider the Detector, at a distance D_2 from the source: the counting rate is $r \sim 700\ \frac{\gamma}{\text{s}}$.

3 Calibration of the Scintillators

Before performing any measurement, it's necessary to properly set the CFD threshold. To estimate the latter, the following procedure is used: connect to the oscilloscope one of the CFD output and the anode signal of the FIFO, while triggering on the former one; varying the threshold value (by means of a screw-driver), it can be seen how the anode signal changes. In particular, when the noise disappears the minimum threshold to cut off the low energy signals is reached. The threshold is then set at that value, namely $V_{thr} \sim 100$ mV.

3.1 Calibration

After the correct setting of the CFD threshold, one can proceed to the calibration of the three detectors. For this purpose, the two gamma rays of the ^{22}Na, at 511 keV and 1275 keV will be exploited. To improve the accuracy of the result, a ^{241}Am source is also used which, emitting a photon at 59 keV, provides a better calibration especially for the low-energy part of the spectra. For what concerns the setup, the detector is set at 0° at a distance D_3 and the Americium source is put between the Scatterer and the Detector. The anode signal from the FIFO of the Detector is sent to channel 1 of the digitizer, while the delayed output of the CFD is sent to the Logic Unit which is set to 'fold 1' since we're not interested in coincidences for the purpose of calibration. The output of the latter module is then connected as the trigger in

[4]Fold N represents the coincidence between N detectors, regardless of the input order.

the digitizer. After checking that the counting rate is similar to the expected value (Section 2) connecting the CFD prompt output to the CAEN scaler, the data acquisition can start. Once acquired the Detector's spectrum, it's possible to fit the three photopeaks with a gaussian function plus a linear one. The described procedure is then performed again for the Tagger and the Scatterer; the mean, standard deviation and the χ^2 of the fits are presented in Table 1, while the spectrum for the Tagger with relative interpolations is depicted in Figure 4. The other uncalibrated spectra are reported in Appendix (Figure 15).

	Peak (keV)	E (a.u.)	σ (a.u.)	$\chi^2/d.o.f.$
TAGGER	59	1075.2 ± 0.2	106.9 ± 0.3	14
	511	8572.0 ± 0.8	282.1 ± 0.7	3.2
	1275	21087 ± 2	474 ± 2	1.5
SCATTERER	59	1164.2 ± 0.6	166.0 ± 0.8	6.4
	511	9327.8 ± 0.7	319.5 ± 0.6	3.5
	1275	22928 ± 2	521 ± 2	1.4
DETECTOR	59	1108.5 ± 0.2	111.9 ± 0.1	94
	511	8680 ± 10	280 ± 10	1.0
	1275	21440 ± 10	440 ± 10	0.94

Table 1: Fitting parameters for the three peaks in the spectrum for each of the detectors.

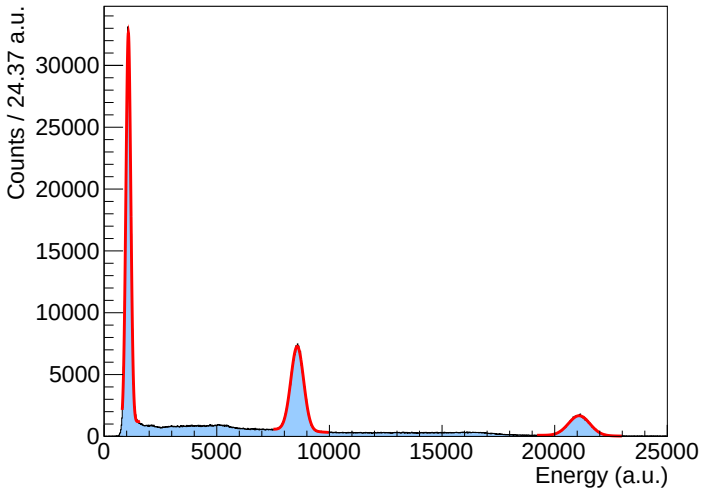

Figure 4: Tagger spectrum with the three gaussian fits

The χ^2 test might underline some problems in the fit procedure for the first peak of the three detectors. This is probably due to the fact that the threshold cuts off the background for low energy and the peak goes sharply to zero, making the fit procedure harder for the software considering the presence of the Compton shoulder right after the gaussian. Despite the χ^2 being far from the expected value, it seems that the mean and the width of the 59 keV resemble quite well the data for all the three detectors. As far as the other two peaks, the presence of similar background (or, at least, that can be interpolated with a linear function in first approximation) to the left and to the right of the gaussian makes the chi-square closer to the theoretical value. Being satisfied with the obtained fit parameters, the centroids can be then associated with the known value of the energy for each photon (respectively 59 keV, 511 keV, 1275 keV [5]) to enable a linear fitting procedure to obtain the calibration curve for each of the detectors; the calibration curve for the Tagger is depicted in Figure 5, while the final linear coefficients for the three detectors are presented in Table 2. The other detector's calibration curve are in the Appendix (Figure 16).

[5]The precise values are: 59.5409 ± 0.0001 keV, 1274.537 ± 0.007 keV, $510.99895000 \pm 0.00000001$ keV. Source: http://www.nucleide.org

It's somehow difficult to establish whether a three-point linear fit is satisfactory, since the residuals cannot show possible systematic trends. On the other hand, the χ^2 test is not really reliable since the errors on the known value of energies are really small, and the same can be said for the errors on the centroid position; this translates to a $\chi^2/d.o.f. \gg 1$ for the Tagger and the Scatterer, while the Detector's test is closer to the unitary value, but still not satisfactory. Nevertheless, the subsequent analysis did not show any issue linked to the position of the peaks in the calibrated spectra, so we can accept the calibration parameters given by the linear fits.

	q (keV)	m ($\frac{\text{keV}}{\text{a.u.}}$)
TAGGER	-5.61 ± 0.02	0.060491 ± 0.000005
SCATTERER	-6.15 ± 0.03	0.055640 ± 0.000004
DETECTOR	-6.68 ± 0.04	0.05974 ± 0.00003

Table 2: Calibration parameters for the three detectors (line equation: $y = q + mx$)

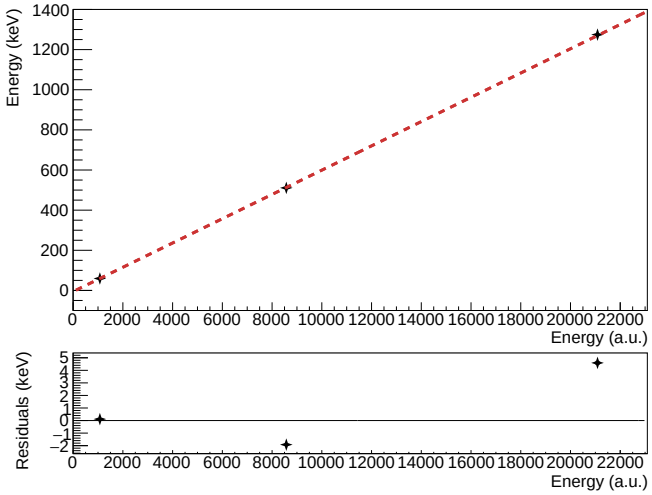

Figure 5: Tagger calibration curve obtained with the gaussians' centroids (above) and residuals of linear fit (below)

3.2 511 keV photopeak analysis

Since it will be useful for the measurement of the cross section, we want to estimate the number of events in the full-energy peak at 511 keV, A_{511}, with respect to the total number of events in the detector A_{tot}, namely $F_{511} = \frac{A_{511}}{A_{\text{tot}}}$. Using an acquisition spectrum for the Tagger with only the ^{22}Na source, A_{511} can be obtained subtracting the Compton background from the range of interest for the photopeak. The procedure is depicted in Figure 6 as the highlighted part of the histogram is the one giving A_{511}. Using as uncertainty on the fraction, $\sigma_{F_{511}} = \sqrt{(\frac{F_{511}}{A_{511}})^2\sigma^2_{F_{A11}} + (\frac{F_{\text{tot}}}{A_{\text{tot}}})^2\sigma^2_{F_{511}}}$ [6] with errors on the integrals given by $\sqrt{N}$ (considering a Poisson statistics), the final result is

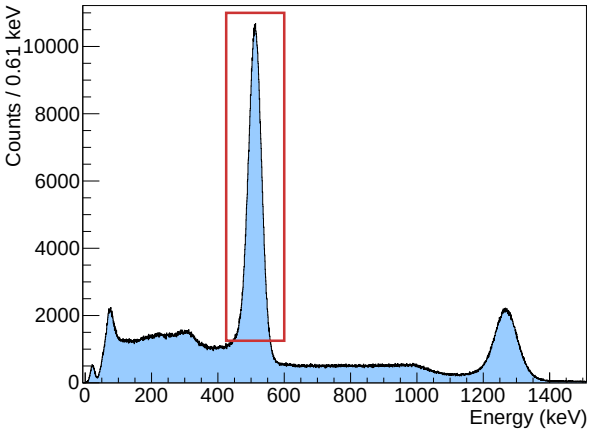

Figure 6: Tagger spectrum with ^{22}Na source. The red box highlights the part of spectrum used to determine A_{511}.

$$F_{511} = (33.49 \pm 0.05)\%$$

[6] Note that, from now on, the uncertainty on a derived quantity will always be obtained with error propagation, meaning $\sigma_f = \sqrt{\sum_i \frac{\partial f}{\partial \Theta_i}^2 \sigma^2_{\Theta_i}}$.

Photopeak resolution It's interesting to analyze the dependence of the resolution of the 511 keV peak on the number of the events in it. In fact, supposing the linearity of the detector response, the average pulse height is $E \propto N$; if the process of revealing a photon follows the Poisson statistics, the variance will be $\sigma^2 \propto N$, namely, $\sigma \propto \sqrt{N}$. Defining the resolution as $R = \frac{\text{FWHM}}{E} = \frac{\sqrt{8 \ln 2}\sigma}{E}$, it can be easily seen that $R \propto \frac{1}{\sqrt{N}}$. Acquiring spectra at different statistics for the tagger, it's possible to verify the previous relation by fitting the peak at 511 kev in order to get the centroid and the sigma of the gaussian. The results with relative fitting fuction are shown in Figure 7 with the x-axis set to $1/\sqrt{N}$ to better visualize the expected trend.

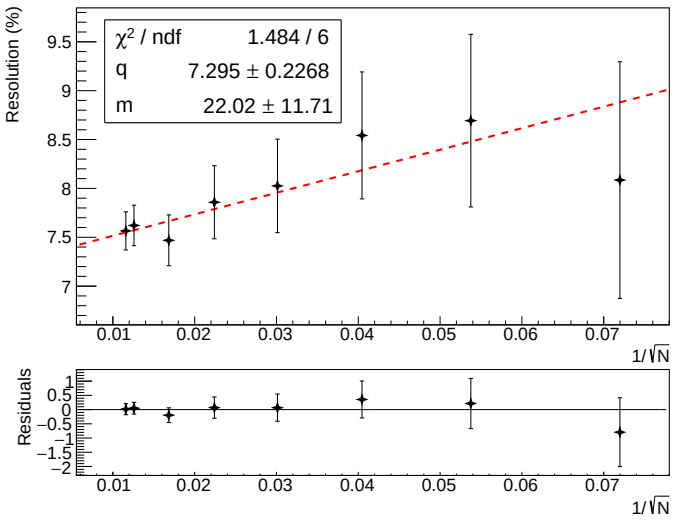

Figure 7: Fit of resolution vs $1/\sqrt{N}$ with residuals for the Tagger detector.

The fit appears to be satisfactory. The residuals do not show any systematic trend and the χ^2 value is good. There might be a slight overestimation of the errors; indeed, for smaller samples the peak is mixed with the background, meaning that the uncertainties on the fit parameters become larger. From these considerations we can conclude that the predicted relation between resolution and number of counts in the peak is verified. Additionally, the plot shows that for $1/\sqrt{N} \lesssim 0.015$ the resolution tends to remain constant with increasing statistics: namely, for $N \gtrsim 1/(0.015)^2 \sim 4500$ the precision cannot increase anymore. Furthermore, knowing the fraction of events in the photopeak with respect to the total spectrum F_{511}, we can conclude that for $N_{\text{total}} = \frac{N}{F_{511}} \gtrsim 14000$ entries in the total spectrum, the maximum resolution is reached.

4 Study of the Scattered Particles

Once the setup has been calibrated, the CFD's delayed output is displayed using the oscilloscope and its width is adjusted to roughly 100 ns. Employing both the oscilloscope's channels, the CFD's outputs linked to each detector are compared in order to find and eventually maximize the overlapping regions. The overlap coincidence is achieved when two signals have a non-null time intersection. At this point, measurements are collected imposing the triple coincidence of Tagger, Scatterer and Detector: it is possible to estimate the acquisition time by checking the events counting rate on the CAEN Quad Scaler module. In order to verify the relation between energy and angle of the diffused photon, spectra of the three detectors are acquired moving the Detector at the angular positions $\theta_i = (0°, 20°, 40°, 60°, 90°)$. The calibrated spectra at $\theta = 90°$ are depicted in Figure 8: the acquisition for this angular position was carried out over three days and therefore represents a much larger sample than the others. The histograms related to the other angles can be retrieved in the Appendix (Figure 17). In the first histogram, the full-energy peak at 511 keV corresponds to the 'tagging photon' emitted by the ^{22}Na source in coincidence with the considered beam. On the Scatterer spectrum, while the full-energy peak is still detected, it should be noted that the first peak represents the scattered electron.

Finally, in the last spectrum the highest peak refers to the scattered photon, whose energy is complementary to the electron energy, approximately adding up to the expected 511 keV. To better understand the correlation between the detectors' spectra, the events of interest have to be selected by means of a software gate.

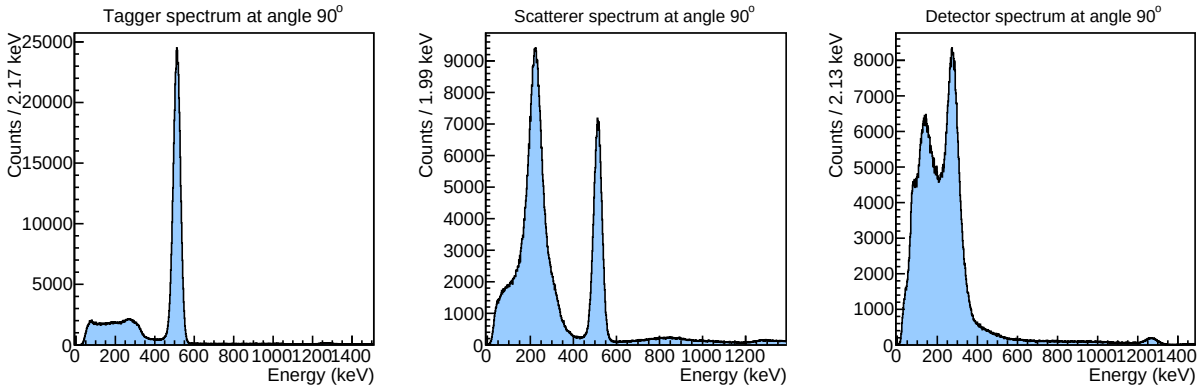

Figure 8: Calibrated spectra related to Tagger, Scatterer and Detector at the angular position $\theta = 90°$.

4.1 Selection of the Compton Events

Firstly, the tagger events are filtered by selecting the $(460 - 560)$ keV range on the calibrated spectrum, namely isolating the full-energy peak. On the other hand, recalling equation (1) and using energy conservation one can obtain

$$E_e = E_i \left(1 - \frac{1}{2 - \cos\theta}\right) \tag{2}$$

in which $E_i = 511$ keV. It is thus possible to retrieve the expected scattered electron's energy E_e at a given angle θ. By adjusting the range around $E_e(\theta_i)$, the valuable events in the Scatterer spectrum are identified. The timestamps linked to the selected events in the Tagger and Scatterer spectra are retrieved and matched, fixing possible broken coincidences. It is worth noting that since the acquisitions are carried out by triggering on the triple coincidence, we expect that the coincident signals all have the same time reference value. The Detector spectrum is filtered by fetching only the events that are in coincidence with both the selected Tagger and Scatterer events: in this way the combination of both the software gates is pushed onto the Detector spectrum. The filtered spectra linked to the angular position $\theta = 90°$ are represented in Figure 9. The histograms for the other angles are in the Appendix (Figure 18).

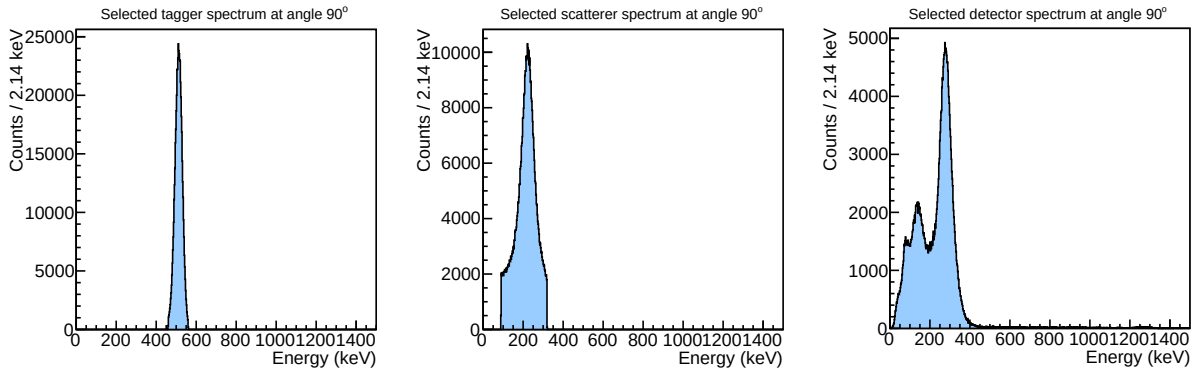

Figure 9: Selected spectra related to Tagger, Scatterer and Detector at the angular position $\theta = 90°$.

Energy Conservation Check An energy conservation check is finally carried out on the Scatterer and Detector events. In particular, two dimensional histograms were filled with coincident

events (selected as previously described) linked to scattered electron and photon, whose energies combined have to sum up to 511 keV within a 5% range (properly selected to optimize the visualization). By imposing this constraint, the Detector versus Scatterer histograms clearly show a strong correlation, rising from the fact that their coincidence was the trigger for the acquisition. The histograms are shown in Figure 10 for the angle $\theta = 90°$; Figure 19 depicts the histograms for the other angular positions.

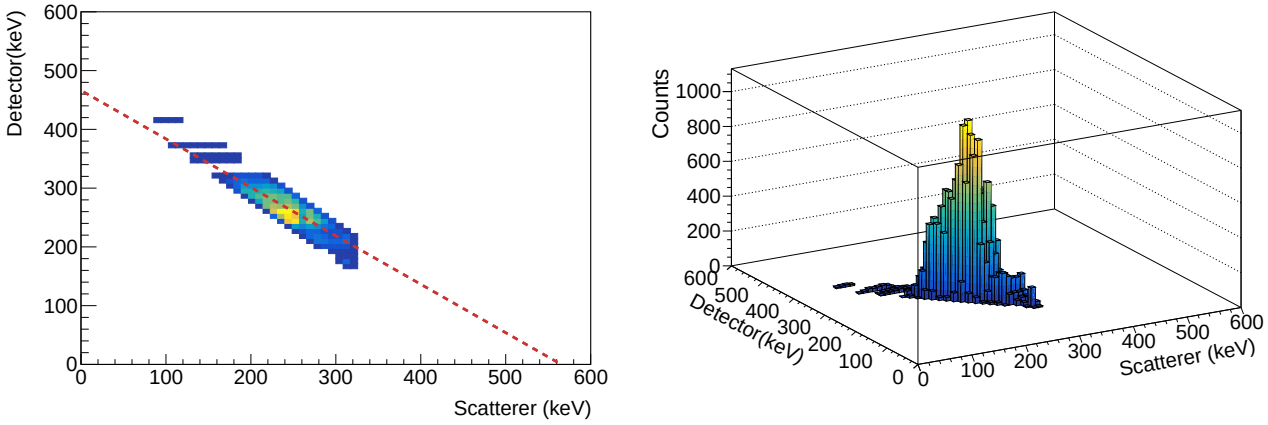

(a) Two dimensional visualization.

(b) Three dimensional visualization.

Figure 10: Multi-dimensional histogram visualizations for Detector with respect to Scatterer for the angle $\theta = 90°$.

To check for the quality of the selection, it is possible to operate a linear fit on the two dimensional histogram. Since the event-by-event energy sum for Detector and Scatterer should add to 511 keV, we expect that the intercepts with both the x-axis and y-axis are roughly equal to 511 keV; on the other hand, the slope should be close to -1. For instance, this is the case for the histogram at $\theta = 90°$, pictured in Figure 10a: the intercepts and slope agree with the expected values within a 15% variation range. This analysis was performed for each angular position. Nevertheless, these interpolations are carried out just as a check for the selection procedure and do not hold any claim to be a parameter estimation procedure. Even if the results are not optimal (especially for angles less than 90°, being the samples smaller), we can conclude that the selection of the Compton events was rather satisfactory.

4.2 Photon and Electron Energy Trends

The spectra of scattered electron and photon are analyzed for each angular position and a Gaussian fit is performed on the selected peaks, in order to determine the energies E_e and E_f. In particular, Figure 11 shows the diffused photon and electron energy trends as function of the Detector's angular position; the trends expected from equations (1) and (2) are also depicted for reference. The dashed lines in Figure 11 represent the fit curves, obtained using equations (1) and (2). The free parameter is in both cases the initial photon energy E_i, which resulted $E_i^{(\gamma)} = 500 \pm 20$ keV and $E_i^{(e)} = 440 \pm 40$ keV, respectively for the photon and electron fit. Both values show a decent compatibility coefficient[7] ($\lambda < 2$) with the expected value $E_i = 511$ keV. Nevertheless, the interpolation is clearly not optimal, starting from the high reduced chi-square, $\chi^2/d.o.f. \gg 1$ in both cases. Moreover, the residuals shown on the right appear to have a systematical parabolic trend, with the point related to $\theta = 0°$ being far off the zero line. This may be due to the fact that for this angular position the electron should have null energy and experimentally this translates into a zero-centred Gaussian. Surely, since the histograms are defined for non negative energies the Gaussian fit at $\theta = 0°$ is not optimal. Indeed, it should be mentioned that the fit trends are close to the expected energy trends.

[7]The *compatibility coefficient* between a known value μ and a generic result $x \pm \sigma_x$ is defined as $\lambda = \frac{|x-\mu|}{\sigma_x}$.

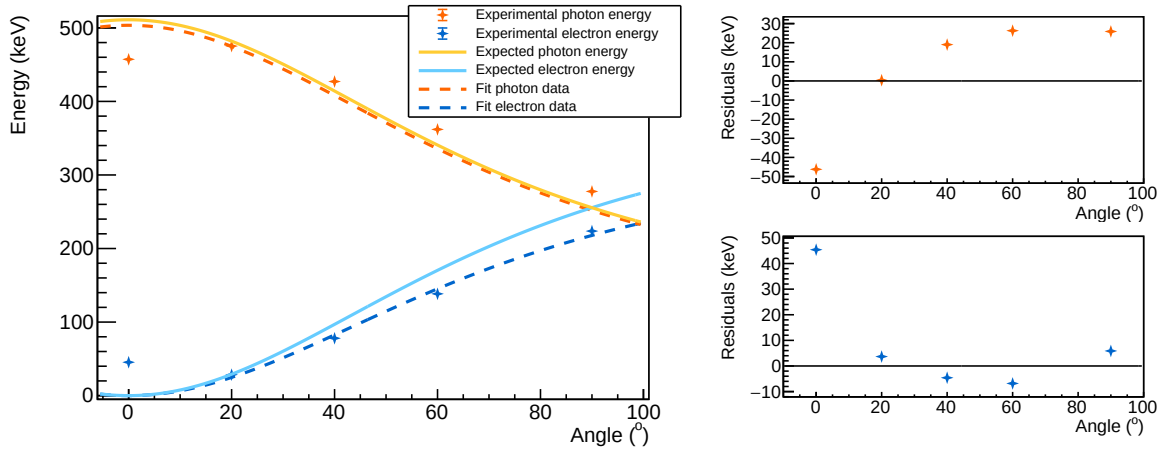

Figure 11: Scattered electron and photon energy trends as function of the angle. Dashed lines are the fits on the experimental data, on the right the residuals are presented.

5 Measurement of the Compton Cross Section

Conclusive part of the data analysis is aimed at estimating the differential cross section of Compton scattering referred to angular position $\theta = 90°$. For the final acquisitions the Scatterer is removed from the experimental setup and is substituted by an aluminum sample. The sample consists of a cylindrical volume of diameter $d = 3.50 \pm 0.04$ cm and thickness $h = 0.80 \pm 0.04$ cm (the estimated volume is $V = 7.7 \pm 0.5$ cm^3). The Detector is fixed at $\theta = 90°$ (maximum angle achievable because of geometric impediment due to lead shield), maintaining the distance from the source as previously imposed.
Two spectra are acquired imposing these condition, one with the ^{22}Na source and a background one, in which the source is removed. Acquisitions are taken with previous settings but, in this case, the coincidence used as trigger is the one between the Tagger and the Detector (LU set to 'fold 2'). During the measurements, the counting rate referred to Tagger is recorded from the CFD in order to later calculate the total number of events registered.

5.1 Experimental cross section esteem

The experimental cross section can now be obtained as:

$$\left[\frac{d\sigma}{d\Omega}\right]_{\text{exp}} = \frac{\Sigma_\gamma}{\epsilon \cdot N \cdot \Delta\Omega_f \cdot \frac{I}{S}} \tag{3}$$

where Σ_γ consists of the amount of events in the full energy peak of Detector spectrum for scattered photons at $\theta = 90°$, ϵ is the photopeak efficiency of the Detector, N represents the number of electrons presented in the aluminum sample, $\Delta\Omega_f$ is the solid angle covered by the Detector and $\frac{I}{S}$ is the number of photons that hit the sample per unit of surface.
The derivation of Σ_γ is performed by first selecting acceptable events recorded in the Tagger spectrum considering an energy range around the 511 keV peak of $(460 - 560)$ keV (10% tolerance). The corresponding Detector events are consequently selected evaluating the relative timestamps (analogously to Section 4.1). To analyze the energy peak around the expected photon energy at $\theta = 90°$, the background spectrum has to be subtracted. The subtraction is applied taking into account the different acquisition times, re-weighting background entries using the time duration of Detector's acquisition. Finally, Σ_γ is obtained by evaluating the integral around the photopeak: the expected photon energy at $\theta = 90°$ is 256 keV, so the range imposed is $(220 - 295)$ keV ($\sim$ 15% tolerance); the achieved result is $\Sigma_\gamma = 1110 \pm 30$. The spectrum's region selected is depicted in Figure 12, where red lines highlight the considered area and 256 keV energy peak can be observed.

In order to deduce the photopeak efficiency ϵ, a spectrum acquisition at angular position $\theta = 0°$ is carried out. The Detector in this case is placed in contact with the source lead collimator: this allows to collect all the tagged photons within Detector angular acceptance. The measurements are acquired using as master gate the coincidence between Tagger and Detector. Both the spectra are recorded: through Tagger spectrum it's possible to calculate the total number of tagged photons, N_{tot}; Detector spectrum, on the other hand, allows to infer the number of events in 511 keV peak, N_1. This last quantity is obtained by eliminating present background, as already applied in Section 3.2. The results are $N_{tot} = 202800 \pm 500$, $N_1 = 123100 \pm 400$. Now, assuming that for each photon hitting the Tagger one is being recorded by the Detector (because of spatial correlation between the two), photopeak efficiency can be expressed as $\epsilon = \frac{N_1}{N_{tot}} = 0.607 \pm 0.002$. Spectra involved in this derivation are presented in Figure 13; the selected area obtained eliminating the background is highlighted in the Detector spectrum.

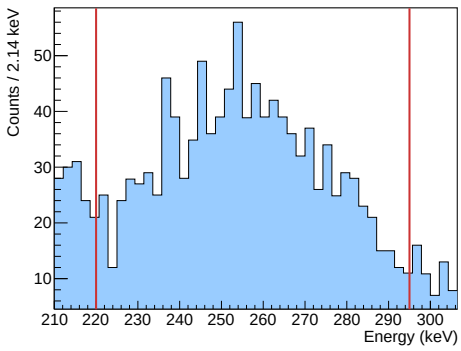

Figure 12: Detector spectrum around scattered photons' peak for $\theta = 90°$ imposing Tagger-Detector coincidence

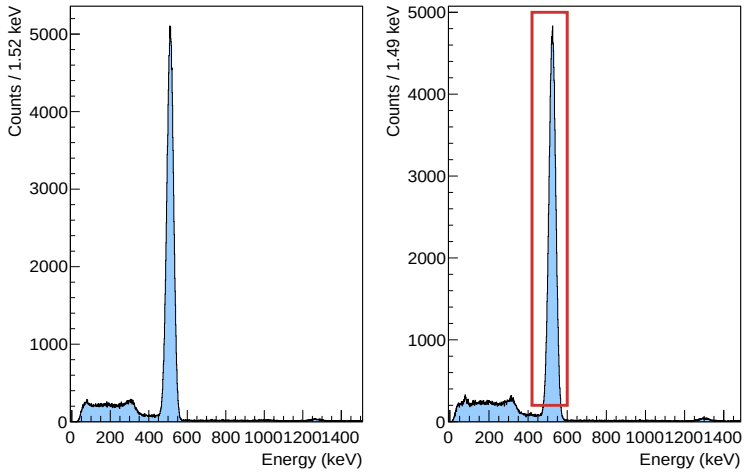

Figure 13: Tagger (left) and Detector (right) spectrum registered with Detector at null distance and at $\theta = 0°$, imposing Tagger-Detector coincidence

The term N can be derived as $N = \frac{V \cdot \rho \cdot N_{Avogadro} \cdot Z}{A_r}$, in which aluminum density $\rho = 2.7$ g/cm^3, atomic number $Z = 13$ and aluminum atomic weight $A_r = 26.98$ $\frac{\text{g}}{\text{mol}}$ are presented. Exploiting the volume V of the sample previously considered, $N = (6.0 \pm 0.4) \times 10^{24}$.
$\Delta\Omega_f$ is estimated through the total surface that the detector covers ($A = \pi(\frac{d_D}{2})^2 = 44.2 \pm 0.9$ cm^2, where $d_D = 7.50 \pm 0.04$ cm is the Detector aperture diameter as anticipated in Section 2) and the known distance between Detector and source, D_2; the angle is then $\Delta\Omega_f = \frac{A}{D_2^2} = 0.032 \pm 0.002$.
Lastly it's possible to deduce the value of I involving the total number of events collected by Tagger: this quantity, N_{scaler}, is obtained considering the product between the counting rate showed by the CAEN scaler display during the acquisitions, as previously described, and the total duration of acquisitions themselves. Thanks to N_{scaler} and the fraction $F(511)$, evaluated in Section 3.2, one can calculate the total number of photons in 511 keV peak that are elaborated by the electronics as $I = N_{\text{scaler}} \cdot F(511) = (7.66 \pm 0.01) \times 10^6$. In this way the number of photons hitting the sample per unit of surface is computed as $\frac{I}{S} = (8.0 \pm 0.4) \times 10^5$ cm^{-2}, remembering that the total surface is $S = \pi(\frac{d}{2})^2 = 9.6 \pm 0.4$ cm^2.
Exploiting all the obtained results, the experimental differential cross section of Compton scat-

tering, referred to angular position $\theta = 90°$ results:

$$\left[\frac{d\sigma}{d\Omega}\right]_{\text{exp}} = (1.18 \pm 0.12) \times 10^{-26}\ \text{cm}^2$$

This result may be compared to the theoretical value obtainable with *Klein-Nishina* formula. The formula estimates the differential Compton scattering cross section in the infinitesimal angle $\mathrm{d}\Omega$. Imposing $\theta = 90°$, it can be calculated:

$$\left[\frac{d\sigma}{d\Omega}\right]_{\text{th},\theta=90°} = \frac{r_e^2}{2}\left(\frac{E_f}{E_i}\right)^2\left(\frac{E_f}{E_i} + \frac{E_i}{E_f} - \sin^2\theta\right)\Bigg|_{\theta=90°} = 1.49 \times 10^{-26}\ \text{cm}^2$$

Angular considerations To justify the discrepancy between the obtained results, it was tried to analyze possible inaccuracies in the supposed angular position ($\theta = 90°$). Since the Detector has a non-zero diameter and spatially covers a geometric surface, the angle imposed can't be experimentally evaluated as a single value. In particular, the angular range covered at fixed position θ is $[\theta - \delta\theta, \theta + \delta\theta]$ with $\delta\theta = \arctan\left(\frac{d_D/2}{D_2}\right) = 5.8°$. One can therefore compute a mean of the expected cross section, integrating Klein-Nishina over this angular range, $(\int_{84.2°}^{95.8°} \frac{d\sigma}{d\Omega}\, d\theta)/2d\theta$. Nevertheless, this calculation essentially coincide with the theoretical result previously evaluated, not justifying the distance between the two values.

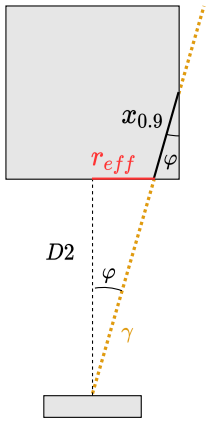

Figure 14: Geometry scheme

Another attempt at explaining the discrepancy was given considering the fact that for angles near $\theta \pm \delta\theta$ the photons can interact with matter only for a very short length, therefore we can approximately consider that, at such angles, the γ rays do not interact with scintillator. That way, one can find an *effective area* for interaction, reducing the value of $\Delta\Omega_f$. Remembering the gamma intensity dependency on distance $I(x) = I_0 e^{-\mu x}$, imposing $I(x_{0.9}) = 0.9 I_0$ (what we can consider a almost non-interacting photon beam) we get $x_{0.9} = 0.05$ cm, distance travelled by the photons to reduce the intensity of 10%, with $\mu \sim 0.2\ \text{cm}^{-1}$ [8]. Looking at the geometry depicted in Figure 14 we can solve graphically the system to find $r_{eff} \sim 3.70$ cm. Therefore, the cross-section with $\Delta\Omega_{eff}$ (solid angle covered by the effective area) becomes: $\frac{d\sigma}{d\Omega} \sim 1.21 \times 10^{-26}\ \text{cm}^2$. The result is not satisfactory, being still far from the expected value, so the former analysis can be discharged like the previous one.

6 Conclusions

After the analysis we can conclude that:

1. the calibration was sufficiently accurate, since the analysis did not show any systematic error in the positions of the calibrated peaks;

2. the selection procedure of the Compton events was rather satisfactory and this led to the verification of the relation between energy of the diffused particles and angle. Nevertheless, the fit over experimental data was not optimal. In particular, the energy at $\theta = 0°$ was quite far from the expected value since the gaussian should have been centered to zero, while our spectra are positive-defined in energy;

[8] Source: https://www.researchgate.net/figure/Linear-attenuation-coefficients-for-solid-curves-LaBr-and-dashed-cu fig3_27345216

3. the value of the experimental cross section at $\theta = 90°$ does not seem compatible with the theoretical one; two attempts were given at reducing the discrepancy with geometrical considerations, but none of them was successful. It's hypothesized that other systematic errors shall be taken into account to justify the results.

7 Appendix

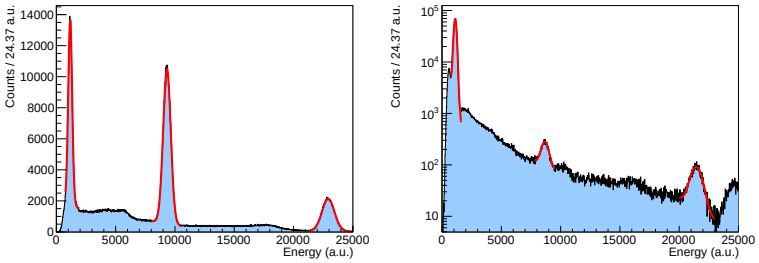

Figure 15: Uncalibrated spectra for Scatterer (left) and Detector (right) with three gaussian fits.

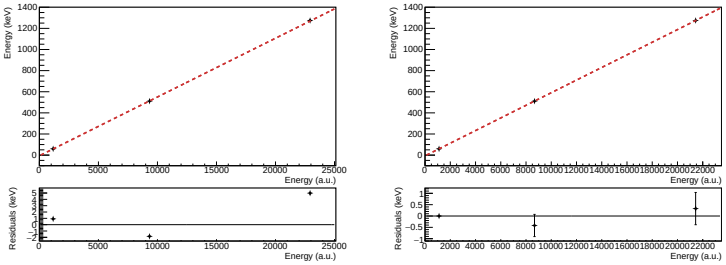

Figure 16: Calibration curves for Scatterer (left) and Detector (right) with relative residuals

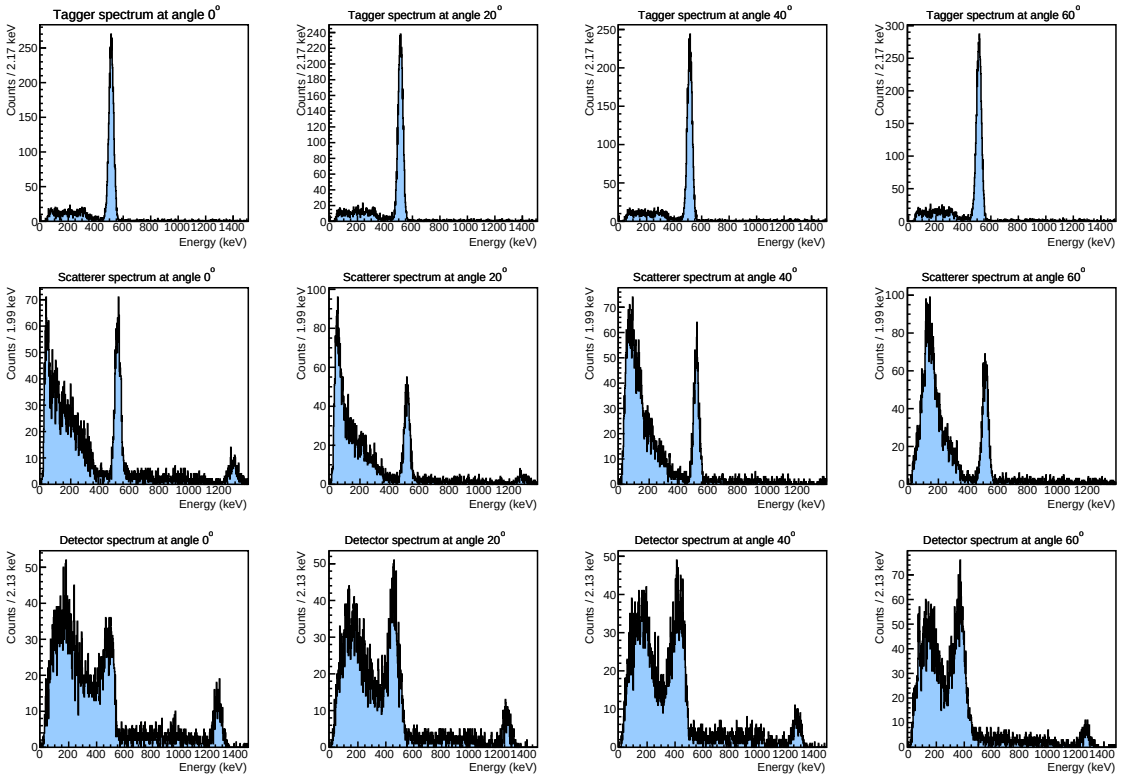

Figure 17: Calibrated spectra related to Tagger, Scatterer and Detector.

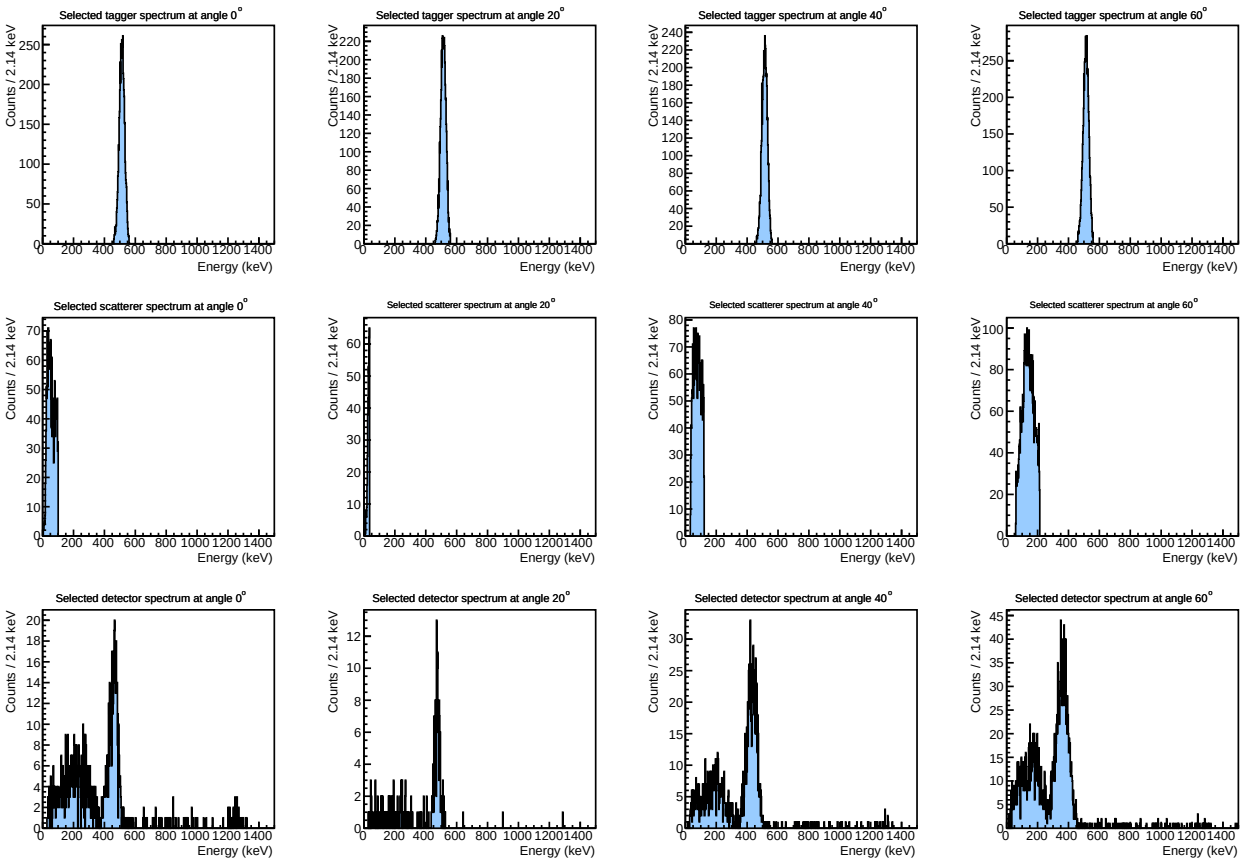

Figure 18: Selected spectra related to Tagger, Scatterer and Detector.

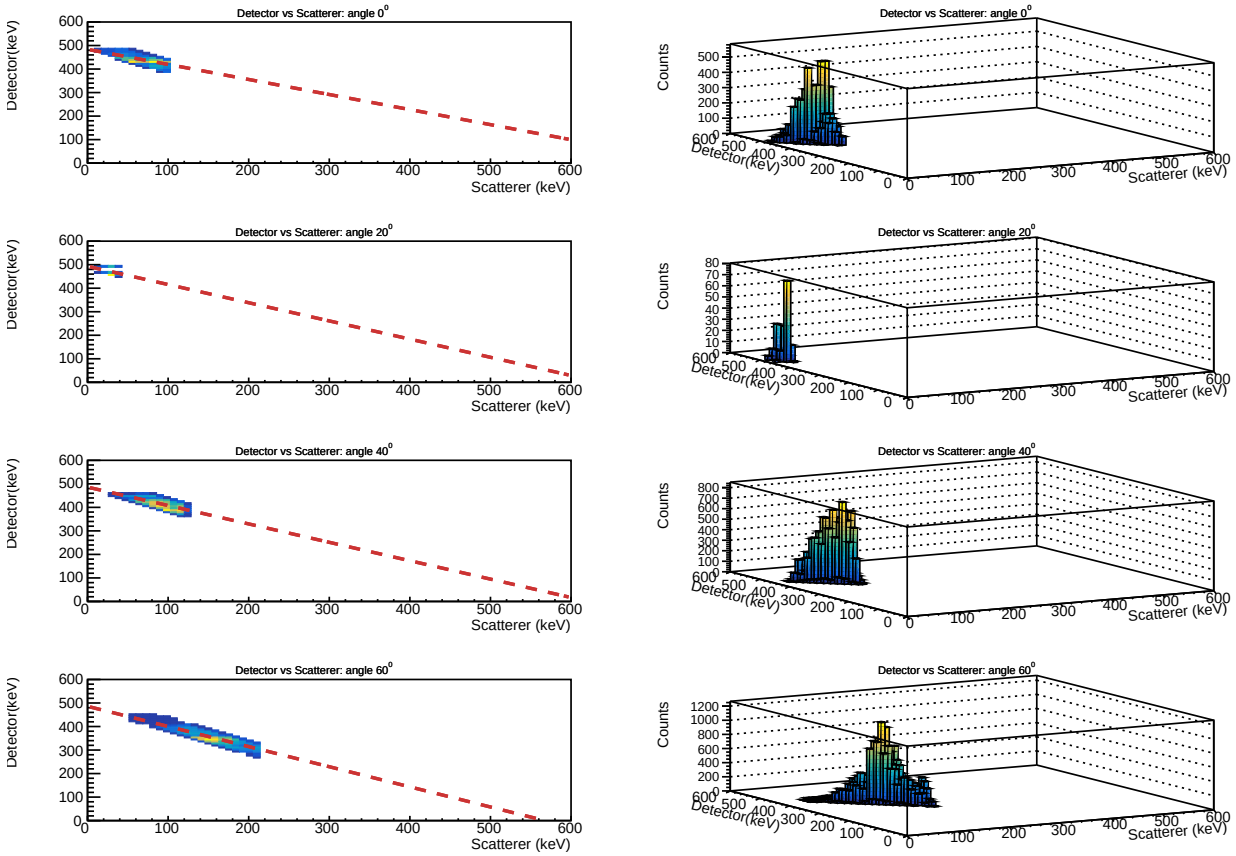

Figure 19: Two and three dimensional histograms of Detector events with respect to Scatterer's.